



How Far Has AI Come in Liver Fibrosis Staging? A Large-Scale Real-World Dataset and Benchmark

Yuanye Liu^a, Nannan Shi^b, Zhejia Zhang^c, Hanxiao Zhang^{d,e}, Boya Wang^f, Derong Yu^g, Nao Wang^h, Yuxin Jinⁱ, Yang Zhou^j, Kunhao Yuan^k, Siqi Wang^l, Lida Yang^m, Xu Qiao^m, Wentao Liu^l, Xuelei Heⁱ, Xin Hong^h, Guoyan Zheng^g, Xin Chen^f, Guang-Zhong Yang^{d,e}, Le Zhangⁿ, Lei Li^o, Yuxin Shi^b, Xiahai Zhuang^{a,*}

^aSchool of Data Science, Fudan University, Shanghai, China

^bDepartment of Radiology, Shanghai Public Health Clinical Center, Fudan University, Shanghai, China

^cDepartment of Electrical and Computer Engineering, Northwestern University, Evanston, USA

^dShanghai Key Laboratory of Flexible Medical Robotics, Tongren Hospital, Institute of Medical Robotics, Shanghai Jiao Tong University, Shanghai, China

^eSchool of Biomedical Engineering, Shanghai Jiao Tong University, Shanghai, China

^fSchool of Computer Science, University of Nottingham, Nottingham, UK

^gInstitute of Medical Robotics, School of Biomedical Engineering, Shanghai Jiao Tong University, Shanghai, China

^hCollege of Computer Science and Technology, Huaqiao University, Xiamen, China

ⁱSchool of Electronic Information (School of Artificial Intelligence), Northwest University, Xi'an, China

^jDepartment of Mechanical Engineering, University College London, London, UK

^kInstitute of Neuroscience and Cardiovascular Research, University of Edinburgh, Edinburgh, UK

^lCAS Center for Excellence in Nanoscience, National Center for Nanoscience and Technology, Beijing, China

^mSchool of Control Science and Engineering, Shandong University, Jinan, China

ⁿSchool of Engineering, College of Engineering and Physical Sciences, University of Birmingham, Birmingham, UK

^oDepartment of Biomedical Engineering, National University of Singapore, Singapore, Singapore

ARTICLE INFO

Article history:

Received 4 May 2024

Received in final form **

Accepted **

Available online **

Communicated by **

2000 MSC: 41A05, 41A10, 65D05, 65D17

Keywords: Liver Fibrosis Staging, Benchmark, Dataset, Medical Image

ABSTRACT

Despite years of methodological progress, how far AI has come in liver fibrosis staging has never been systematically evaluated under the heterogeneous, multi-center conditions that define clinical practice. To address this gap, we introduce LiFS (Liver Fibrosis Staging), a large-scale dataset and benchmark derived from the MICCAI 2025 CARE-Liver challenge, comprising 610 patients across multiple centers and scanners with multi-sequence MRI (T1W, T2W, DWI, and four-phase gadoteric acid-enhanced imaging). To the best of our knowledge, LiFS is the first benchmark providing complete gadoteric acid-enhanced sequences with histopathology-confirmed annotations from diverse real-world scanners. Through systematic evaluation of 9 independently developed methods selected from 96 registered teams against in-cohort radiologist reference results, our findings address how far current AI has progressed toward clinical-level liver fibrosis staging from three complementary perspectives. First, against radiologists, the best AI methods were broadly comparable to the senior radiologist and significantly exceeded the junior radiologist in selected settings, while median AI performance generally approached junior-radiologist levels. Second, from a data perspective, cross-center heterogeneity, label imbalance, and contrast-enhanced sequence variability emerge as the dominant challenges for AI methods. In particular, the hepatobiliary phase offers valuable functional information but also introduces cross-center variability, creating a practical dilemma in its use and calling for standardized acquisition and generalization-aware modeling. Third, from a technical perspective, methodological design choices, including spatial registration, input dimensionality, multi-modal fusion strategy, and backbone architecture, appear to modulate cross-center robustness, although no single choice alone closes the gap. Overall, LiFS provides a rigorous real-world benchmark for positioning the current state of AI in liver fibrosis staging and for enabling future research on the key challenges that limit clinically reliable deployment.

1. Introduction

Artificial intelligence (AI) has demonstrated remarkable potential in medical image analysis, and liver fibrosis staging from MRI is no exception. Over the past decade, deep learning methods have achieved impressive results on this task, with leading approaches reporting high diagnostic accuracy on curated benchmarks (Yasaka *et al.*, 2017). Yet most existing methods are developed and tested in controlled settings, rather than in the heterogeneous multi-scanner environments encountered in real clinical practice (Nowak *et al.*, 2021; Zhao *et al.*, 2024). A fundamental question thus remains unanswered: how far has AI actually come in staging liver fibrosis clinically? This paper provides a systematic answer through LiFS, a large-scale, multi-center dataset and benchmark designed to evaluate the current status of AI.

Liver fibrosis, characterized by excessive extracellular matrix deposition leading to architectural distortion, is a critical stage in the progression of chronic liver disease (Bataller *et al.*, 2005), and accurate staging is essential for identifying patients at risk of advancing to cirrhosis or hepatocellular carcinoma (HCC) (Asrani *et al.*, 2019; Roehlen *et al.*, 2020). The current gold standard, histopathological examination via liver biopsy, is invasive and subject to sampling variability (Bravo *et al.*, 2001; Rockey *et al.*, 2009), motivating the search for non-invasive alternatives. Magnetic resonance imaging (MRI) offers detailed soft tissue contrast through multiple complementary sequences (T1W, T2W, DWI) (Jackson *et al.*, 1997), and gadoteric acid-enhanced (GED) imaging further provides hepatocyte-specific functional information critical for fibrosis characterization (Ahn *et al.*, 2010; Lohrke *et al.*, 2016), with representative LiFS examples shown in Fig. 1. Deep learning has shown strong potential for automating staging from such multi-sequence data (Liu *et al.*, 2025b), but progress has been constrained by the absence of large-scale, multi-center benchmarks that capture real clinical complexity.

Existing datasets for liver MRI remain limited in scale, sequence coverage, or annotation scope (Table 1): none currently provides the combination of multi-center acquisition, complete gadoteric acid-enhanced (GED) sequences including the hepatobiliary phase (HBP), and histopathology-confirmed fibrosis staging labels needed to evaluate AI under realistic conditions. Prior benchmarks have focused primarily on segmentation rather than staging, and have not systematically assessed robustness to cross-center domain shift or multi-modal integration challenges.

To address these gaps, we introduce LiFS, a large-scale benchmark derived from the CARE-Liver challenge held in conjunction with MICCAI 2025¹, designed to evaluate AI algorithms under authentic clinical conditions. Through systematic evaluation of 9 independently developed methods selected from 96 registered teams on LiFS, this work directly examines a single core question that, to the best of our knowledge, has

never been addressed in a unified real-world benchmark: *how far has current AI progressed toward clinical-level liver fibrosis staging?* We approach this question from three complementary angles:

- (1) *AI versus clinical experts.* How does the diagnostic performance of current AI methods compare with that of practicing radiologists on the same real-world MRI cases, under both matched acquisition conditions and cross-center distribution shifts?
- (2) *Data-perspective challenges.* What data-side factors, including cross-center heterogeneity, label imbalance, and contrast-enhanced sequence variability, limit AI performance under real clinical conditions?
- (3) *Technical-perspective challenges.* Which methodological design choices, including input dimensionality, multi-modal fusion strategy, spatial registration, and backbone architecture, appear associated with robustness under realistic acquisition conditions?

To support this investigation, our contributions are as follows. We introduce LiFS, the first large-scale multi-center dataset featuring complete gadoteric acid-enhanced sequences and histopathology-confirmed Scheuer fibrosis grades (Scheuer, 1991) from diverse real-world scanners, enabling rigorous evaluation of cross-center generalization. Building on LiFS, we establish a comprehensive benchmark that examines the core question from the three angles introduced above, anchored by a clinical reference framework that compares AI methods against in-cohort radiologist performance on the same cases. Finally, through in-depth analysis of the nine selected methods, we provide empirically grounded insights spanning all three angles: AI’s clinical readiness relative to radiologists, the data-side factors that limit real-world deployment (cross-center heterogeneity, label imbalance, and contrast-enhanced sequence variability), and the technical design choices associated with robust performance under heterogeneous acquisition conditions.

2. Related Work

2.1. Related datasets

Several public datasets have been established to support research in liver imaging, particularly for tasks like segmentation and disease assessment using MRI. These resources vary in scale, diversity, and annotation types, but most focus on segmentation rather than explicit fibrosis staging, and they often lack the real-world heterogeneity needed for robust algorithm development. For instance, the Duke Liver Dataset (Macdonald *et al.*, 2023) comprises 2146 MRI series (including T1W, T2W, DWI, arterial, and portal-venous phases) from 105 patients, many with cirrhotic features. It provides segmentation annotations for the liver but omits fibrosis staging labels and the critical hepatobiliary phase in the contrast-enhanced protocol, limiting its utility for staging tasks. Similarly, CirrMRI600+ (Jha *et al.*, 2025) includes 628 high-resolution abdominal MRI scans (310 T1W and 318 T2W, with some portal-venous phase data) from 339 patients with liver cirrhosis, offering segmentation

*Corresponding author
e-mail: zzh@fudan.edu.cn (Xiahai Zhuang)

¹https://zmic.org.cn/care_challenges/

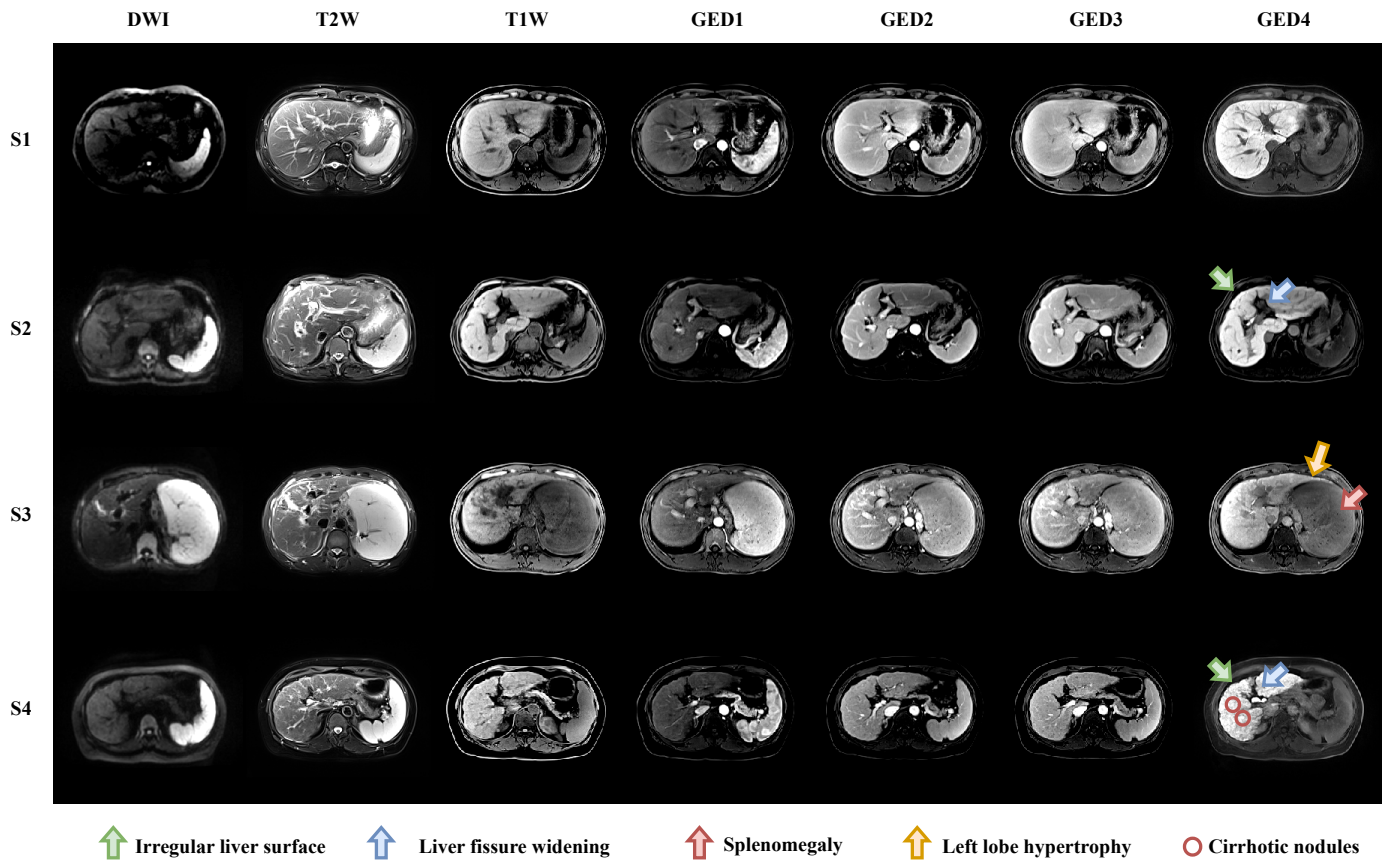


Fig. 1. Sample images from the LiFS dataset demonstrating the four fibrosis stages (S1-S4) across seven MRI sequences. Each row represents one fibrosis stage, and each column shows a different MRI sequence: Diffusion-Weighted Imaging (DWI), T2-weighted (T2W), T1-weighted (T1W), and four dynamic phases of gadoteric acid-enhanced (GED1–4) imaging (arterial, portal venous, delayed, and hepatobiliary phases, respectively). Representative fibrosis signs in the GED4 (HBP) column are highlighted with arrows and circles to illustrate characteristic imaging features at each stage.

Table 1. Comparison of LiFS with existing liver-related MRI datasets. LiFS stands out as the largest multi-center dataset featuring comprehensive GED sequences and histopathology-confirmed fibrosis staging labels. Abbreviations: HBP, hepatobiliary phase; Art., arterial phase; PV, portal venous phase; Del., delayed phase; 3-class, three-class fibrosis grading system; Seg., segmentation.

Dataset	Patients	Volumes	Multi-center	NonContrast Seq.	Contrast Seq.	Fibrosis Staging	Segmentation	Venue
Duke Liver (Macdonald et al., 2023)	105	2,146	✓	T1W, T2W, DWI	Art., PV	✗	Liver Seg.	Online
CirrMRI600+ (Jha et al., 2025)	339	628	✗	T1W, T2W	PV	✓(3-class)	Liver Seg.	Online
LiverHccSeg (Gross et al., 2023)	46	~184	✗	T1W	Art., PV, Del.	✗	Tumor/Liver Seg.	Online
CHAOS (Kavur et al., 2021)	40	120	✗	T1W, T2W	✗	✗	Organ Seg.	ISBI 2019
LiFS (Ours)	610	4,174	✓	T1W, T2W, DWI	GED (incl. HBP)	✓(S1-S4)	Liver Seg.	MICCAI 2025

masks. However, it is derived from a single center, lacks comprehensive multi-phase GED imaging, and does not include multi-modal sequences like DWI. Other notable datasets include LiverHccSeg (Gross et al., 2023), which provides multi-phase MRI (arterial, portal-venous, delayed phases) from 46 patients with HCC, annotated for liver and tumor segmentation but without fibrosis staging. Broader multi-organ MRI datasets like CHAOS (Kavur et al., 2021) offer T1W and T2W scans from 40 subjects for abdominal organ segmentation, but they are small-scale, single-center, and not tailored to liver fibrosis or cirrhosis. Table 1 summarizes these comparisons, highlighting how LiFS advances the field with its larger cohort, multi-center acquisition, extensive multi-sequence coverage (including four GED phases), and dedicated fibrosis staging annotations. This enables more realistic benchmarking for non-invasive diagnos-

tic models.

2.2. Methods for MRI-based liver fibrosis staging

Deep learning has been applied to liver fibrosis staging across multiple imaging modalities, including ultrasound (Lee et al., 2020; Xue et al., 2020), computed tomography (Choi et al., 2018; Yasaka et al., 2018), and histopathology (Wojciechowska et al., 2021; Yin et al., 2024). Among these, MRI is particularly attractive owing to its rich tissue contrast and ability to capture functional information without ionizing radiation. Early MRI-based approaches relied on single sequences such as T2W combined with transfer learning (Nowak et al., 2021), while subsequent works demonstrated the superior diagnostic value of gadoteric acid-enhanced HBP images (Yasaka et al., 2017; Hectors et al., 2021). More recent frameworks integrate T1W,

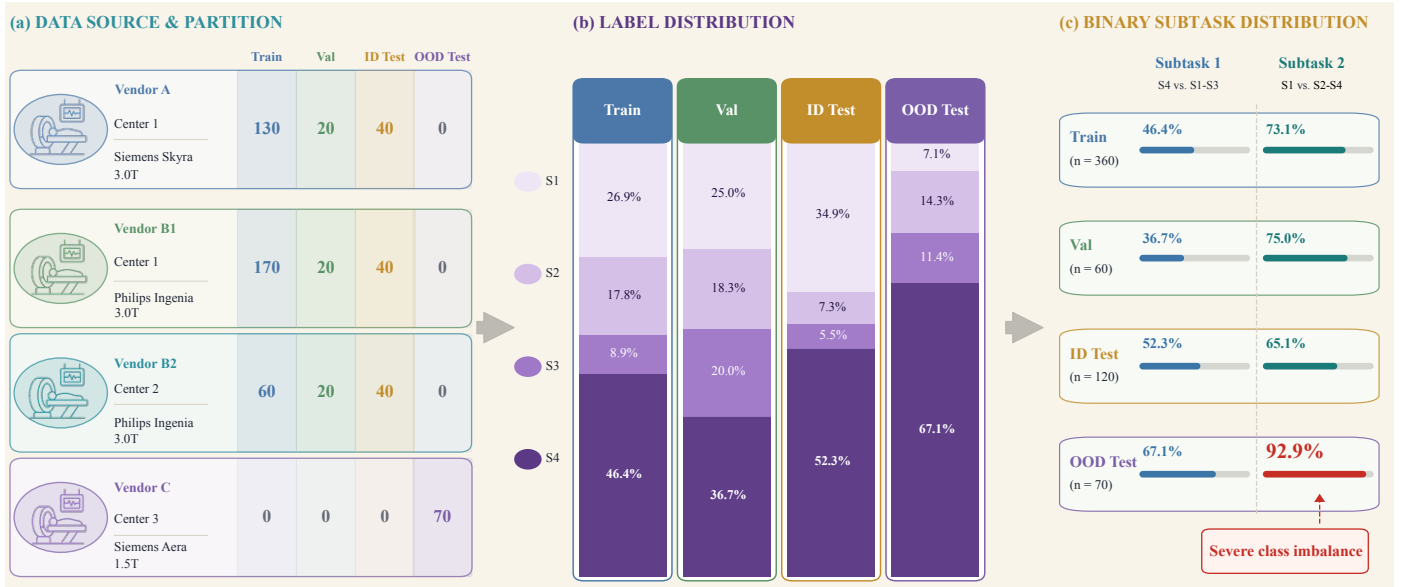


Fig. 2. Overview of the LiFS dataset. (a) Data collection and partitioning across multiple centers and vendors. (b) Class distribution of fibrosis stages across training, validation, and test sets. (c) Binary Subtask Label distribution across train, validation and test sets.

T2W, DWI, and contrast-enhanced phases (Zheng *et al.*, 2024; Li *et al.*, 2024; Zhao *et al.*, 2024), sometimes fusing clinical metadata with imaging features (Li *et al.*, 2025). Interpretable architectures, such as multi-view evidential learning, have also been explored for this task (Gao *et al.*, 2023; Liu *et al.*, 2025a).

However, existing methods have been developed predominantly under controlled, single-center conditions with full-modality availability. Systematic evaluation of cross-center generalization remains largely absent (Zheng *et al.*, 2024), and interpretability-focused approaches have not been tested under distribution shift. LiFS aims to fill this gap by providing a unified evaluation platform that exposes the discrepancy between laboratory performance and real-world clinical requirements.

3. LiFS: A Multi-Modality Liver Fibrosis Staging Dataset

3.1. Overview

We release LiFS, a large-scale, open-access dataset for liver fibrosis staging that reflects real-world clinical complexity. The dataset includes 610 patients from multiple centers, scanned with multi-sequence, contrast-enhanced liver MRI. In total, LiFS contains 4,174 3D MRI volumes (in NIfTI format) and 218,203 slices. The training and validation subsets, including annotations, are publicly available at https://zmic.org.cn/care_c_challenges/.

As summarized in Fig. 2, data were collected from three clinical centers and four different MRI scanners, covering both 1.5T and 3.0T magnetic field strengths. Vendor A and Vendor B (two centers, three scanners) provided 360 and 60 subjects for training and validation, respectively, while Vendor C (one independent scanner) served exclusively as the out-of-distribution (OOD) test set with 70 patients, used to assess model generalization. All cases were derived from real clinical environments, and therefore may contain coexisting liver lesions, such as HCC.

The MRI acquisition protocol followed the standard multi-phase dynamic contrast-enhanced sequence: the arterial phase is captured approximately 25 seconds after contrast injection, followed by the portal venous phase (after 1 minute), delayed phase (after an additional 90 seconds), and finally the HBP acquired 20 minutes post-injection. HBP has been shown to provide functional liver signals most informative for fibrosis characterization.

Ground-truth was determined by histopathological examination from biopsy or surgical resection performed within three months of the MRI scan, ensuring clinical consistency and reliability. Fibrosis stages were defined according to the Scheuer grading system (Scheuer, 1991): S1 (fibrous portal expansion), S2 (bridging fibrosis), S3 (fibrosis with architectural distortion), and S4 (cirrhosis).

3.2. Real-world features

LiFS was designed to replicate the real-world challenges encountered in clinical MRI data analysis, providing a comprehensive platform for developing robust and generalizable algorithms. Key characteristics include: (1) Spatial Misalignment: The multi-sequence MRI volumes (T1W, T2W, DWI, GED1–4) are not spatially registered, reflecting routine acquisition variability in clinical workflows. (2) Missing Modalities: Certain subjects lack one or more sequences due to acquisition failure, motion artifacts, or protocol variations, making LiFS suitable for evaluating modality-robust learning and modality completion methods. (3) Cross-center Heterogeneity and Generalization: Data were collected from three hospitals and four scanners using different vendors and field strengths, introducing domain shifts that test the cross-site generalization ability of learning algorithms.

It is worth noting that the HBP, acquired approximately 20 minutes post-injection, is particularly susceptible to inter-center

Table 2. Summary of participants and submitted methods in the LIFS benchmark. VOI = Volume of Interest; ROI = Region of Interest; CNN = Convolutional Neural Network.

Team	Institute	Data	Method	Training	GitHub Repo
SJTU1	Shanghai Jiao Tong University	Dim: Cropped Located VOI (3D) Fusion: Late Fusion (Average)	Pre-segmentation: Used for VOI cropping Generalization: Additional pretrain	Backbone: ResNet-34 (CNN) Device: NVIDIA 3090	https://github.com/Hanx-Zhang/Liver-Fibrosis-Quantification-and-Analysis
UoB	University of Birmingham	Dim: Whole Volume (3D) Fusion: Middle fusion (Attention)	Label imbalance: Stratified sampling Generalization: Soft voting ensemble Modality missing: Synthetic compensation	Backbone: mmFormer (Transformer) Device: NVIDIA A100	https://github.com/zhangzhejia2002-1gfm/Delta-mmFormer
UoN	University of Nottingham	Dim: Cropped Located Patch (2D) Fusion: Early fusion (Patch-based)	Pre-segmentation: Used for ROI cropping Label imbalance: Augmentation Pre-registration: Rigid registration Modality missing: Zero matrix	Backbone: ResNet-18 (CNN) Device: NVIDIA RTX A6000	https://github.com/mileywang3061/Care-Liver
SJTU2	Shanghai Jiao Tong University	Dim: Overlapping Volume (3D) Fusion: Middle fusion (Attention)	Label imbalance: Weighted cross-entropy Modality missing: Random Dropout Train	Backbone: Anatomix (CNN) Device: NVIDIA Tesla H100	https://github.com/Kendra9999/MA2
SDU	Shandong University	Dim: Whole Volume (3D) Fusion: Middle fusion (feature)	Pre-segmentation: Used for VOI cropping Modality missing: Zero matrix	Backbone: ALMSS (CNN) Device: NVIDIA A100	https://github.com/LidaiY412/34-LIFS
NCTST	National Center for Nanoscience and Technology	Dim: Whole Volume (3D) Fusion: Middle fusion (feature)	Pre-registration: ✓ Modality missing: Zero matrix	Backbone: UniFormer (Transformer) Device: NVIDIA RTX 8000	https://github.com/WWangSiqi/Multi-branch-attention-Network
HQU	Huaqiao University	Dim: Compressed Volume (2D, described as 2.5D in paper) Fusion: Middle fusion (feature)	Label imbalance: Focal Loss Modality missing: Zero matrix	Backbone: Swin Transformer Device: NVIDIA RTX 4090	https://github.com/hxpotato/CARE2025
NWU-CN	Northwest University	Dim: Cropped Located Patch (2D) Fusion: Late fusion (attention gating)	Pre-segmentation: Used for ROI cropping Generalization: Uncertainty-guided curriculum learning	Backbone: ResNet-18 (CNN) Device: NVIDIA RTX 4090	https://github.com/pazjini/FIBUCL
UCL	University College London	Dim: Handcrafted Features (32D) Fusion: Middle fusion	Pre-segmentation: Used for ROI cropping Pre-registration: Rigid Generalization: Additional scanner flag	Backbone: Random Forest Device: AMD Ryzen 5 5600 & NVIDIA A100	https://github.com/YangForever/care2025_liver_bioreamer

variability. Differences in injection protocols, patient liver function, and scanner characteristics may substantially alter HBP signal intensity across sites, introducing domain shifts that are qualitatively distinct from those observed in routine anatomical sequences. This property makes LiFS uniquely suited to evaluate whether AI methods can robustly exploit functional hepatobiliary information across heterogeneous acquisition environments.

3.3. Research opportunities

To the best of our knowledge, LiFS is the largest annotated multi-sequence MRI dataset for liver fibrosis staging to date. Its scale, diversity, and real-world imperfections open a wide range of research directions, including but not limited to: (1) Multi-modality fusion and representation learning; (2) Domain generalization and adaptation across centers and vendors; (3) Missing-modality reconstruction and modality-agnostic inference; (4) Robustness and uncertainty estimation for clinical reliability. We welcome the community to explore and build upon LiFS to advance the development of reliable, interpretable, and clinically applicable AI for liver disease assessment.

4. CARE-Liver Challenge

4.1. Challenge set-up

The CARE Challenge was held in conjunction with MICCAI 2025, aiming to address the comprehensive challenges inherent to real-world clinical deployment. Among all tasks, the CARE-Liver track focuses on liver MRI, comprising two tasks: LiFS and Liver Segmentation (LiSeg). For LiFS, we established two experimental tracks: (1) Contrast-Enhanced, utilizing all available sequences (T1W, T2W, DWI, and GED1–4); and (2) Non-Contrast, restricted to T1W, T2W, and DWI sequences to assess performance without exogenous agents. Two clinically important subtasks, Cirrhosis Detection (S4 vs. S1–3) and Significant Fibrosis Detection (S1 vs. S2–S4) (Choi *et al.*, 2018), were evaluated.

In this challenge, 96 teams registered, 220 evaluations were submitted, and 13 papers were accepted in the workshop proceeding (Zhuang *et al.*, 2025). For LiFS, nine teams submitted final results on the test set. Table 2 summarizes the participating teams, their affiliations, the main design characteristics of their methods, and the availability of released code repositories.

4.2. Evaluation

We evaluated all methods on both in-distribution (ID) and OOD test sets. The ID test data were drawn from the same distribution as the training set, whereas the OOD test data came from a completely unseen scanner and clinical center (Vendor C), enabling assessment of cross-domain generalization.

The primary evaluation metrics were classification accuracy (ACC) and area under the receiver operating characteristic (ROC) curve (AUC). ACC reflects overall classification correctness, while AUC provides a threshold-independent measure of discriminative ability, which is particularly important under label imbalance.

In addition to the nine challenge submissions, we implemented two baselines, ResNet3D (He *et al.*, 2016) and ViT3D (Dosovitskiy *et al.*, 2021), to provide standardized reference models under a controlled training protocol. Both baselines were trained by the organizers using the same official training and validation partitions as the challenge participants and were evaluated on the same ID and OOD test sets.

Radiologist annotation. To establish an in-cohort clinical reference, two board-certified radiologists with 3 and 8 years of abdominal imaging experience (denoted Expert-3Y and Expert-8Y, respectively) served as in-cohort clinical readers and independently evaluated the same LiFS benchmark cases using a 7-point qualitative MRI scoring scheme (Venkatesh *et al.*, 2015). Cases were presented in two separate reading sessions, with an independently randomized case order in each session. In the first session, all benchmark cases were assessed using only the non-contrast sequences (T1W, T2W, DWI). In the subsequent session, the same cases were assessed under the contrast-enhanced setting after revealing the GED1–4 sequences. Both radiologists were blinded to the histopathological ground truth, patient clinical information, the other radiologist’s scores, and the train/validation/test partition (including the ID/OOD designation). The two readings were retained strictly as separate references (Expert-3Y and Expert-8Y); no averaging or consensus reconciliation was performed. Because the radiologist ratings were ordinal, AUC was used as the primary metric for comparison with AI methods, retaining the ranking information of the 7-point scores.

AI-versus-radiologist significance testing. Significance analysis was performed separately for each evaluation cell defined by acquisition setting (contrast-enhanced or non-contrast), domain (ID or OOD), and binary subtask. All comparisons were conducted on the case-aligned cohort shared by all official AI submissions and the two radiologists. Within each cell, official team submissions were ranked by AUC. Best AI was defined as the submission with the highest AUC, and Median AI was defined as the median-ranked submission. Their AUCs were compared with each radiologist using the paired DeLong test for correlated ROC curves (DeLong *et al.*, 1988). Statistical significance was reported at a nominal threshold of $\alpha = 0.05$.

4.3. Methodological overview

As summarized in Table 2, the nine submitted methods exhibit a diverse array of strategies tailored to the challenges of liver fibrosis staging. We categorize these contributions along three primary dimensions: input representation and backbone architecture, multi-modal fusion strategy, and mechanisms for handling real-world heterogeneity.

Input Representation and Backbone Architecture. Volumetric 3D approaches were the predominant choice, adopted by five teams (SJTU1, UoB, SJTU2, SDU, NCTST) to exploit global contextual information from the liver MRI. In contrast, 2D patch-based networks (UoN, NWU-CN) focused on capturing fine-grained local textural details, while Team HQU employed a 2.5D compression strategy to balance spatial context

Table 3. Comprehensive performance comparison for the Liver Fibrosis Staging (LiFS) benchmark. The table merges results for Contrast-enhanced and Non-contrast MRI settings across In-Distribution (ID) and Out-of-Distribution (OOD) datasets. Subtask 1 and Subtask 2 denote (S4 vs. S1-3) and (S1 vs. S2-4), respectively. Best results for each setting are highlighted in bold, and the second-best performances are underlined. Results shaded in grey indicate evaluations conducted after the conclusion of the challenge. Bottom rows summarize the radiologist reference reading (Expert-3Y/8Y) and the per-endpoint best/median AI; values are AUC. Expert-3Y and Expert-8Y denote radiologists with 3 and 8 years of experience, respectively. Subscripts indicate the corresponding team. Superscript arrows denote exploratory paired DeLong test results for AUC comparison on the same test cases. \uparrow 3Y indicates that the displayed AI AUC was significantly higher than Expert-3Y with unadjusted $p < 0.05$. \downarrow 8Y indicates that the displayed AI AUC was significantly lower than Expert-8Y with unadjusted $p < 0.05$.

Team	Contrast-Enhanced								Non-Contrast							
	ID				OOD				ID				OOD			
	Subtask 1		Subtask 2		Subtask 1		Subtask 2		Subtask 1		Subtask 2		Subtask 1		Subtask 2	
	ACC	AUC	ACC	AUC	ACC	AUC	ACC	AUC	ACC	AUC	ACC	AUC	ACC	AUC	ACC	AUC
ResNet3D	51.67	71.09	70.00	72.24	32.86	55.41	92.86	54.77	65.00	77.81	73.33	76.01	41.43	62.16	61.43	51.08
ViT3D	65.83	73.43	70.83	72.29	32.86	60.87	84.29	66.46	70.00	74.99	63.33	67.64	64.29	63.64	81.43	36.62
UCL	68.33	77.19	74.58	78.11	63.71	<u>67.40</u>	92.86	47.68	70.83	77.89	70.00	77.11	32.86	56.65	88.29	59.40
SJTU2	70.83	75.10	75.00	78.45	41.43	46.81	64.29	52.62	71.67	78.61	70.00	73.70	42.86	49.31	70.00	31.08
NWU-CN	47.50	78.03	65.83	78.20	32.86	64.11	92.86	52.62	47.50	79.78	65.83	67.27	32.86	46.25	92.86	40.31
UoN	75.83	<u>83.92</u>	77.50	<u>83.42</u>	58.57	54.12	92.86	<u>75.38</u>	70.00	77.22	65.00	74.28	71.43	<u>69.47</u>	92.86	86.31
HQU	69.17	73.77	74.17	79.47	<u>64.29</u>	50.23	92.86	52.31	72.50	77.22	71.67	<u>78.51</u>	<u>70.00</u>	71.51	67.14	33.23
UoB	67.50	71.85	<u>78.33</u>	78.14	74.29	73.54	91.43	79.69	66.67	71.73	74.17	68.48	64.29	68.83	91.43	<u>71.38</u>
SDU	72.50	80.62	75.00	76.57	54.29	61.05	92.86	54.46	75.00	83.76	72.50	68.94	55.71	68.73	92.86	70.15
NCTST	72.50	78.31	80.83	84.50	41.43	66.05	82.86	37.23	<u>74.49</u>	79.94	<u>73.11</u>	78.96	48.57	58.74	92.86	60.00
SJTU1	75.83	86.16	75.00	77.00	48.57	49.40	87.14	68.62	74.17	<u>82.12</u>	69.17	76.32	48.57	45.42	85.71	64.92
Expert/AI	Contrast-Enhanced								Non-Contrast							
	ID (AUC)				OOD (AUC)				ID (AUC)				OOD (AUC)			
	Subtask 1		Subtask 2		Subtask 1		Subtask 2		Subtask 1		Subtask 2		Subtask 1		Subtask 2	
	ACC	AUC	ACC	AUC	ACC	AUC	ACC	AUC	ACC	AUC	ACC	AUC	ACC	AUC	ACC	AUC
Expert-3Y	73.63	76.51	63.88	52.46	69.53	69.76	54.81	64.31	69.53	69.76	54.81	64.31	54.81	64.31	54.81	64.31
Expert-8Y	81.83	80.07	66.65	71.38	77.29	74.96	77.57	78.92	77.29	74.96	77.57	78.92	77.57	78.92	77.57	78.92
Median AI	78.03 _{NWU-CN}	78.20 _{NWU-CN}	61.05 _{SDU}	52.62 _{SJTU2}	78.61 _{SJTU2}	74.28 _{UoN}	58.74 _{NCTST} ^{↓8Y}	60.00 _{NCTST}	78.61 _{SJTU2}	74.28 _{UoN}	58.74 _{NCTST} ^{↓8Y}	60.00 _{NCTST}	58.74 _{NCTST} ^{↓8Y}	60.00 _{NCTST}	58.74 _{NCTST} ^{↓8Y}	60.00 _{NCTST}
Best AI	86.16 _{SJTU1} ^{↑3Y}	84.50 _{NCTST}	73.54 _{UoB}	79.69 _{UoB} ^{↑3Y}	83.76 _{SDU} ^{↑3Y}	78.96 _{NCTST}	71.51 _{HQU}	86.31 _{UoN}	83.76 _{SDU} ^{↑3Y}	78.96 _{NCTST}	71.51 _{HQU}	86.31 _{UoN}	71.51 _{HQU}	86.31 _{UoN}	71.51 _{HQU}	86.31 _{UoN}

with computational efficiency. Notably, one team (UCL) utilized handcrafted radiomics features (32D) rather than deep feature extraction, serving as a classical baseline. Regarding backbone architectures, a transition towards Transformer-based models is observed, with three teams deploying advanced architectures such as mmFormer (Zhang et al., 2022), UniFormer (Li et al., 2023), and Swin Transformer (Liu et al., 2022) to capture long-range dependencies, while others relied on established CNN baselines like ResNet (He et al., 2016) and Anatomix (Dey et al., 2025).

Multi-modal Fusion Strategy. Effective integration of multi-sequence MRI is critical for this task. Middle-level fusion emerges as the dominant strategy (adopted by 6 teams), typically utilizing attention mechanisms or cross-modal modules to interactively learn sequence-level features. Early fusion was employed by UoN, concatenating modality channels or patches at the input stage to learn joint representations from raw data. Conversely, late fusion strategies (SJTU1, NWU-CN) aggregated modality-wise predictions via averaging or gating mechanisms, prioritizing independent feature extraction before final decision-making.

Handling Real-world Challenges. Participants introduced specific modules to address the intrinsic data imperfections

of the LiFS benchmark. (1) *Spatial Misalignment*: To mitigate the lack of pixel-wise alignment across sequences, three teams (UoN, NCTST, UCL) explicitly incorporated rigid registration as a pre-processing step. (2) *Missing Modalities*: To ensure robustness against incomplete scans, several methods incorporated modality-agnostic training strategies. These included zero-padding (UoN, SDU, HQU), random modality dropout during training (SJTU2), and synthetic compensation (UoB). (3) *Generalization & Imbalance*: Advanced learning paradigms were explored to enhance OOD generalization, such as uncertainty-guided curriculum learning (NWU-CN) and soft voting ensembles (UoB). Furthermore, label imbalance was addressed through stratified sampling (UoB), weighted cross-entropy (SJTU2), and focal loss (HQU).

5. Results

5.1. AI methods vs. clinical reference: how far has AI progressed toward radiologist-level performance?

To evaluate current AI progress relative to clinical references on the LiFS benchmark, we compared their performance across acquisition conditions (Contrast-Enhanced and Non-Contrast) and ID/OOD evaluation settings, and contextualized the results

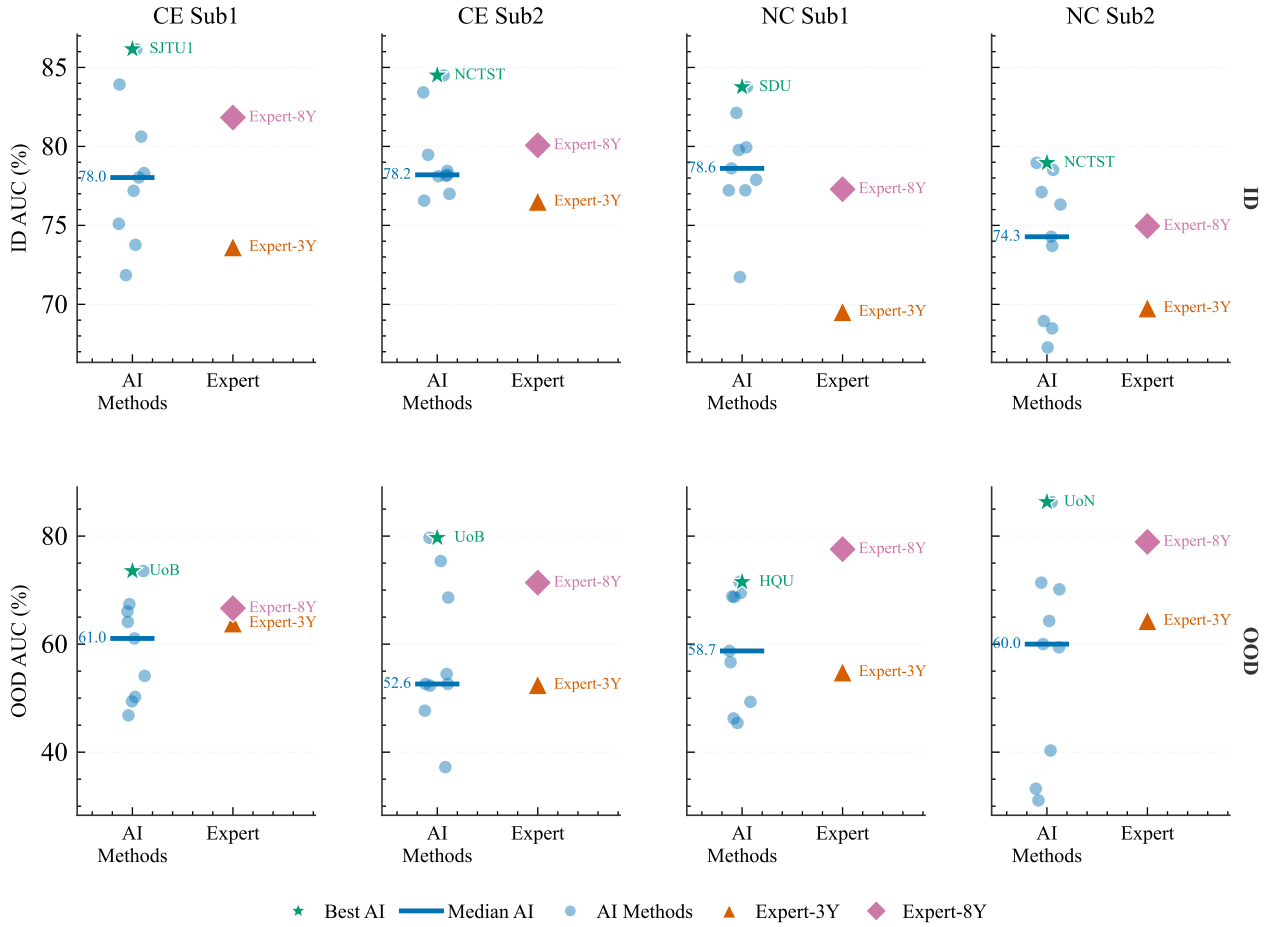


Fig. 3. AUC comparison between radiologists and AI teams across ID/OOD and contrast-enhanced/non-contrast settings. Each blue circle represents an individual AI team, the horizontal bar indicates the median AI performance, and the star highlights the best AI performance. Red triangles and gold diamonds represent Expert-3Y and Expert-8Y, respectively. The plot illustrates both the best-case AI performance and the dispersion of AI results relative to in-cohort radiologist references. Expert-3Y and Expert-8Y denote radiologists with 3 and 8 years of experience, respectively.

with an in-cohort reading by two radiologists with different experience levels (Table 3). The leading method varies substantially across acquisition settings and domains, indicating that no single AI strategy dominates the benchmark. For example, SJTU1 achieved the highest Contrast-Enhanced ID AUC for Subtask 1, reaching 86.16%, but its performance dropped markedly on the corresponding OOD test set, with AUC decreasing to 49.40%. Conversely, UoN showed strong robustness in the Non-Contrast OOD setting, achieving the highest AUC of 86.31% for Subtask 2.

As detailed in Section 4.2 (Radiologist annotation), the in-cohort reference reading by Expert-3Y and Expert-8Y is reported on the 7-point ordinal scale, with AUC as the primary metric for AI-versus-radiologist comparison on the case-aligned cohort; significance annotations are summarized in Table 3.

As shown in Table 3 and Fig. 3, the best-performing AI methods achieved strong performance under ID evaluation, with AUCs above the Expert-3Y reference and in the range of the Expert-8Y reference across all four ID settings. In the contrast-enhanced setting, the best AI achieved AUCs of 86.16 and

84.50 for Subtask 1 and Subtask 2, respectively, compared with 73.63/76.51 for Expert-3Y and 81.83/80.07 for Expert-8Y. A similar pattern was observed in the non-contrast setting, where the best AI achieved AUCs of 83.76 and 78.96, again placing it around the senior-radiologist reference and above the junior-radiologist reference. These results suggest that, under matched acquisition conditions, leading AI methods can reach a senior-radiologist-comparable level, with statistically significant gains over the junior radiologist in selected endpoints. Median AI performance was generally closer to the junior-radiologist reference, indicating that clinical-level performance is not yet consistent across methods.

Under OOD evaluation, the comparison was more heterogeneous. In the contrast-enhanced setting, the best AI achieved AUCs of 73.54 and 79.69, remaining comparable to the senior-radiologist reference and above the junior-radiologist reference for both subtasks. In the non-contrast setting, the best AI achieved the highest AUC for Subtask 2 (86.31), whereas the senior radiologist achieved the highest AUC for Subtask 1 (77.57), exceeding the best AI result of 71.51. The median AI performance also decreased under OOD evaluation, from 78.03

to 61.05 in contrast-enhanced Subtask 1, from 78.20 to 52.62 in contrast-enhanced Subtask 2, from 78.61 to 58.74 in non-contrast Subtask 1, and from 74.28 to 60.00 in non-contrast Subtask 2. These findings indicate that although top AI methods can be comparable to senior-radiologist performance in several settings and significantly exceed the junior radiologist in selected endpoints, this clinical proximity remains sensitive to distribution shift, acquisition setting, and diagnostic endpoint.

5.2. Data-perspective challenges in real-world deployment

To investigate what drives AI's loss of clinical-level performance under realistic conditions, we examined three data-side factors that emerged from the LiFS benchmark: cross-center distribution shift, label imbalance in evaluation, and the variable behavior of contrast-enhanced sequences.

OOD Generalization. As illustrated in Fig. 4(a), most participating methods experienced substantial performance degradation when transitioning from ID to OOD test sets. For example, for SJTU2, the OOD ACC for Subtask 1 dropped from 70.83% to 41.43%, while for Subtask 2 it declined from 75.00% to 64.29%. However, Team UoB showed the smallest aggregate ID-OOD gap and even improved under several OOD endpoints, particularly in the contrast-enhanced setting. This relatively robust generalization may be partly attributable to its synthetic compensation strategy, which synthesizes proxy features for missing modalities from available sequences rather than using zero-padding, potentially preserving multi-modal feature continuity under distribution shift. The soft voting ensemble may further reduce instance-level sensitivity under OOD conditions.

Label Imbalance. Fig. 4(b) plots the relationship between ACC and AUC metrics for all methods on the OOD test set. The analysis reveals a notable discrepancy between ACC and AUC metrics for Subtask 2, where several methods achieved ACC exceeding 85% while their AUC remained below 80%. In contrast, Subtask 1 shows relatively stronger ACC-AUC agreement, whereas Subtask 2 exhibits a more evident discrepancy between high ACC and modest or low AUC. This pattern is consistent with the severe majority-class dominance in Subtask 2, where S2–S4 cases constitute approximately 92.9% of the OOD test set, shown in Fig. 2(c). As shown in Table 3, the recurring ACC value of 92.86% across multiple methods in Subtask 2, particularly paired with low AUCs, strongly indicates model collapse, where algorithms default to predicting the majority class. This confirms that ACC is an unreliable metric for this benchmark due to the skewed distribution. These findings underscore the importance of reporting multiple evaluation metrics, particularly AUC, which provides a more reliable assessment of model discriminative ability when class distributions are imbalanced.

Contrast-Enhanced Sequences. We further explored the impact of including contrast-enhanced sequences on liver fibrosis staging performance. Fig. 4(c) illustrates the performance change from Non-Contrast to Contrast-Enhanced settings for each team under both ID and OOD conditions for Subtask 1 (S4 vs. S1–3). Under ID conditions, the inclusion of GED sequences yielded only marginal performance changes, with AUC fluctuations remaining below 5% for the majority of teams and

the largest improvement being a modest 6.7% (Team UoN). This suggests that standard non-contrast sequences (T1W, T2W, DWI) already provide sufficient discriminatory features when training and test distributions are well-aligned. Moreover, several teams (SJTU1, UoB, HQU, SDU) experienced performance degradation, which may reflect a form of hidden distribution shift intrinsic to the contrast-enhanced phases themselves, especially the HBP. Under OOD conditions, however, the effect of contrast enhancement becomes far more pronounced, yet in opposite directions for different methods. Team NWU-CN and Team UCL achieved substantial AUC improvements of 17.9% and 10.8%, respectively, consistent with the hypothesis that HBP signals capture functional liver information that is more invariant to scanner-induced shifts than anatomical texture. In stark contrast, Team HQU and Team UoN suffered severe OOD degradation of -21.3% and -15.4% , respectively. Overall, these results suggest that contrast-enhanced imaging, especially HBP, provides valuable functional information, but its performance impact varies across methods and evaluation settings, highlighting a practical dilemma in its use under cross-center evaluation.

5.3. Technical-perspective challenges

To examine which methodological design choices are associated with robustness under domain shift, we further explored the technical factors underlying model generalization across acquisition settings. We analyzed four key factors — pre-registration, input dimensionality, fusion strategy, and backbone architecture — and interpreted each in light of the generalization challenges identified above. Results are summarized in Fig. 4(d), where we used an aggregate benchmark score. For each method and each domain (ID or OOD), the aggregate score was computed as the average over all acquisition settings (contrast-enhanced and non-contrast), both binary subtasks, and both evaluation metrics (ACC and AUC).

Pre-registration. The spatial alignment of multi-sequence MRI emerges as a notable preprocessing factor. Methods incorporating pre-registration achieved higher ID performance, with a mean score of $75.99 \pm 1.79\%$ ($n = 3$), compared to non-registered approaches ($73.28 \pm 3.80\%$, $n = 6$). This observation is consistent with the view that pixel-level alignment may be an important prerequisite for effective multi-modal learning, helping fusion modules capture complementary physiological signals rather than noise from anatomical mismatch. For contrast-enhanced sequences, where spatial heterogeneity is compounded by temporal acquisition gaps, the absence of registration may partly explain why some methods were harmed rather than helped by the inclusion of GED sequences.

Input Dimensionality. A clear trade-off between contextual richness and generalization is observed across input dimensionalities. 3D volumetric approaches achieved higher ID performance ($75.33 \pm 2.28\%$) than 2D patch-based methods ($72.23 \pm 5.23\%$), benefiting from the global capture of anatomical context across the liver volume. However, 3D models suffered a substantially larger performance drop ($11.62 \pm 11.08\%$) compared to 2D models ($7.35 \pm 5.83\%$). We hypothesize that 3D networks, in learning to exploit global volumetric structure,

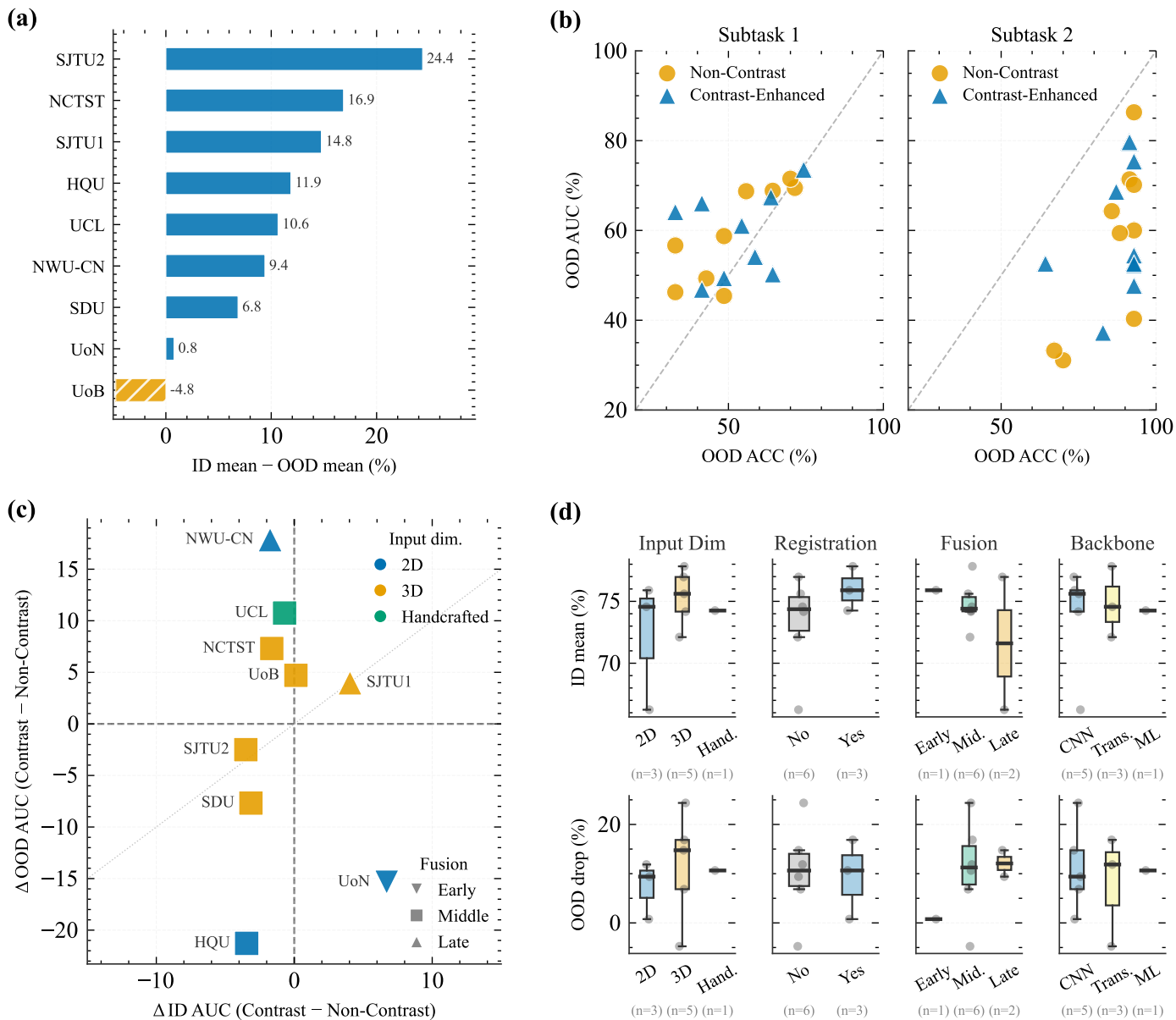


Fig. 4. Comprehensive analysis of challenge results across multiple dimensions. (a) The ID-OOD performance gap reveals substantial generalization challenges. (b) ACC-AUC discrepancy indicates label imbalance effects in Subtask 2. (c) Contrast-enhanced sequences show method-dependent effects under OOD conditions. (d) Factor-wise analysis identifies key design choices affecting model generalization.

inadvertently overfit to vendor-specific spatial priors present in the training data, such as scanner-dependent slice thickness, field-of-view characteristics, and inter-slice spacing, which do not generalize to unseen scanners. 2D models, by focusing on local texture and benefiting from inherent translation invariance, appear less susceptible to these geometric domain shifts. Notably, the handcrafted feature-based approach (UCL) maintained competitive ID performance (74.26%) with moderate OOD drop (10.65%), suggesting that domain-agnostic feature engineering remains a viable strategy, particularly in settings where scanner variability is high and training data is limited. This observation further supports the view that the generalization challenge in LiFS is not unique to deep learning, but reflects a fundamental property of the task.

Fusion strategy. The choice of fusion strategy appears to influence both ID performance and OOD robustness. Early fusion, such as concatenating multi-sequence inputs at the channel level, achieved the highest ID score (75.90%) and the smallest OOD drop (0.77%) among all strategy categories, as demonstrated by Team UoN ($n = 1$). One possible interpretation is that joint representation learning, in which all sequences are processed together from the input stage, encourages the model to learn inter-modality correlations tied to shared anatomy rather than sequence-specific features that may shift across domains. In contrast, late fusion methods, which combine modality-wise predictions at the decision level, achieved the lowest ID performance ($71.61 \pm 7.59\%$) and the largest OOD degradation ($12.08 \pm 3.79\%$), suggesting that independent per-

sequence feature extractors may be more susceptible to domain-specific patterns. Middle fusion, the most prevalent strategy ($n = 6$), yielded a balanced profile (ID: $74.76 \pm 1.89\%$; OOD drop: $10.97 \pm 9.79\%$) but with high variance, reflecting the heterogeneity of attention-based mechanisms across teams. The advantage of early fusion is consistent with the hypothesis that robust multi-modal learning benefits from joint reasoning about sequences, a property that may be particularly relevant when sequences such as HBP introduce their own domain-specific variability.

Backbone architecture. We compared CNN-based backbones against transformer-based architectures across the submitted methods. CNN-based backbones demonstrated comparable ID performance to transformer-based approaches ($73.78 \pm 4.33\%$ vs. $74.83 \pm 2.87\%$). Notably, transformer-based methods exhibited smaller OOD degradation ($7.99 \pm 11.32\%$) compared to CNN-based methods ($11.23 \pm 8.90\%$), suggesting that the ability of the attention mechanism to capture long-range dependencies may confer advantages in handling domain shifts. This pattern is also supported by our additional volumetric baselines, compared with ResNet3D, ViT3D achieved slightly higher aggregated ID performance and a noticeably smaller OOD drop under the same evaluation protocol. These findings indicate that while CNNs remain effective for medical image analysis, transformer architectures hold promise for improving cross-domain generalization in multi-center settings, particularly when sufficient training data is available to mitigate the risk of overfitting.

6. Discussion and Conclusion

This LiFS benchmark was designed to answer a central question: how far has current AI progressed toward clinical-level liver fibrosis staging from real-world MRI? The results suggest that AI has made meaningful progress, but that clinical-level performance remains conditional. Under acquisition conditions similar to the training data, leading AI methods can approach the performance range of experienced radiologists, and in selected exploratory comparisons they exceeded the junior radiologist. This performance pattern suggests that MRI-based AI has the potential to support non-invasive fibrosis staging and, with further prospective validation, may help reduce reliance on biopsy in selected clinical scenarios. However, the same level of performance was not consistently maintained across centers, acquisition settings, and diagnostic subtasks. Median AI performance was generally less competitive, and cross-center evaluation exposed substantial instability. Therefore, the current frontier is not simply achieving high performance on matched test data, but establishing whether learned fibrosis-related imaging patterns remain reliable under heterogeneous clinical acquisition.

The comparison with radiologists helps define this gap in clinically interpretable terms. Human radiologists likely draw on anatomical context, sequence quality, known imaging signs, and prior clinical experience when interpreting fibrosis-related changes. Current AI systems may be more vulnerable to scanner-dependent intensity patterns, texture statistics, or dataset-specific spatial cues. This difference explains why

strong in-distribution performance alone is insufficient evidence for clinical readiness. In its present form, AI appears promising as a decision-support tool under quality-controlled and center-aware deployment, but robust cross-center staging still requires further validation.

Beyond the AI versus radiologist comparison, LiFS also identifies the major data-side and technical challenges that must be addressed for reliable liver fibrosis staging. On the data side, these include cross-center acquisition heterogeneity, label imbalance, and the variable contribution of contrast-enhanced sequences, especially the HBP. On the technical side, the benchmark highlights the need for more robust spatial alignment, multi-modal fusion, missing-modality handling, and architecture design under domain shift. Since the submitted methods differ in multiple coupled design choices, these technical observations should be interpreted as hypothesis-generating and further examined through controlled ablation studies and prospective multi-center validation.

Overall, LiFS shows that MRI-based AI has reached a clinically meaningful level in selected settings, suggesting its potential to support non-invasive liver fibrosis staging and, with further prospective validation, to help reduce reliance on biopsy in selected clinical scenarios. At the same time, its robustness remains insufficient for reliable deployment across heterogeneous clinical environments. By combining multi-center MRI, complete gadoteric acid-enhanced sequences, histopathology-confirmed labels, in-cohort radiologist references, and independently developed challenge submissions, LiFS provides a realistic benchmark for assessing how far AI has progressed in liver fibrosis staging. Importantly, it exposes the gap between strong benchmark performance and clinically reliable AI, and offers a unified platform for studying the key challenges that still limit deployment, including cross-center generalization, imbalance-aware evaluation, robust use of contrast-enhanced imaging, and uncertainty-aware multi-modal modeling. In this sense, LiFS aims to measure current progress while guiding the next stage of research toward reliable, clinically deployable AI for liver fibrosis assessment.

Acknowledgement

This work was funded by the Science and Technology Commission of Shanghai Municipality (25TS1412100), the Non-communicable Chronic Disease-National Science and Technology Major Project (2026ZD0555800/2026ZD0555802), and the National Natural Science Foundation of China (62372115).

References

- Ahn, S.S., Kim, M.J., Lim, J.S., Hong, H.S., Chung, Y.E., Choi, J.Y., 2010. Added value of gadoteric acid-enhanced hepatobiliary phase mr imaging in the diagnosis of hepatocellular carcinoma. *Radiology* 255, 459–466.
- Asrani, S.K., Devarbhavi, H., Eaton, J., Kamath, P.S., 2019. Burden of liver diseases in the world. *Journal of hepatology* 70, 151–171.
- Bataller, R., Brenner, D.A., et al., 2005. Liver fibrosis. *The Journal of Clinical Investigation* 115, 209–218.
- Bravo, A.A., Sheth, S.G., Chopra, S., 2001. Liver biopsy. *New England Journal of Medicine* 344, 495–500.

- Choi, K.J., Jang, J.K., Lee, S.S., Sung, Y., Shim, W., Kim, H., Yun, J., Choi, J.Y., Lee, Y., Kang, B.K., Kim, J., Kim, S., Yu, E., 2018. Development and validation of a deep learning system for staging liver fibrosis by using contrast agent-enhanced ct images in the liver. *Radiology* 289 3, 688–697.
- DeLong, E.R., DeLong, D.M., Clarke-Pearson, D.L., 1988. Comparing the areas under two or more correlated receiver operating characteristic curves: A nonparametric approach. *Biometrics* 44, 837–845.
- Dey, N., Billot, B., Wong, H.E., Wang, C.J., Ren, M., Grant, P.E., Dalca, A.V., Golland, P., 2025. Learning general-purpose biomedical volume representations using randomized synthesis, in: *Proceedings of the International Conference on Learning Representations (ICLR)*.
- Dosovitskiy, A., Beyer, L., Kolesnikov, A., Weissenborn, D., Zhai, X., Unterthiner, T., Dehghani, M., Minderer, M., Heigold, G., Gelly, S., et al., 2021. An image is worth 16x16 words: Transformers for image recognition at scale, in: *Proceedings of the International Conference on Learning Representations (ICLR)*.
- Gao, Z., Liu, Y., Wu, F., Shi, N., Shi, Y., Zhuang, X., 2023. A reliable and interpretable framework of multi-view learning for liver fibrosis staging, in: *Proceedings of the International Conference on Medical Image Computing and Computer Assisted Intervention (MICCAI)*.
- Gross, M., Arora, S., Huber, S., Kücükçaya, A.S., Onofrey, J.A., 2023. Liverhccseg: A publicly available multiphase mri dataset with liver and hcc tumor segmentations and inter-rater agreement analysis. *Data in Brief* 51, 109662.
- He, K., Zhang, X., Ren, S., Sun, J., 2016. Deep Residual Learning for Image Recognition, in: *Proceedings of the IEEE/CVF Conference on Computer Vision and Pattern Recognition (CVPR)*, pp. 770–778.
- Hectors, S.J., Kennedy, P., Huang, K.H., Stocker, D., Carbonell, G., Greenspan, H., Friedman, S., Taouli, B., 2021. Fully automated prediction of liver fibrosis using deep learning analysis of gadoxetic acid-enhanced mri. *European radiology* 31, 3805–3814.
- Jackson, E.F., Ginsberg, L.E., Schomer, D.F., Leeds, N.E., 1997. A review of mri pulse sequences and techniques in neuroimaging. *Surgical Neurology* 47, 185–199.
- Jha, D., Susladkar, O.K., Gorade, V., Keles, E., Antalek, M., Seyithanoglu, D., Cebeci, T., Aktas, H.E., Kartal, G.D., Kaymakoglu, S., et al., 2025. Large scale mri collection and segmentation of cirrhotic liver. *Scientific Data* 12, 896.
- Kavur, A.E., Gezer, N.S., Barış, M., Aslan, S., Conze, P.H., Groza, V., Pham, D.D., Chatterjee, S., Ernst, P., Özkan, S., et al., 2021. Chaos challenge-combined (ct-mr) healthy abdominal organ segmentation. *Medical Image Analysis* 69, 101950.
- Lee, J.H., Joo, I., Kang, T.W., Paik, Y.H., Sinn, D.H., Ha, S.Y., Kim, K., Choi, C., Lee, G., Yi, J., et al., 2020. Deep learning with ultrasonography: automated classification of liver fibrosis using a deep convolutional neural network. *European radiology* 30, 1264–1273.
- Li, C., Wang, Y., Bai, R., Zhao, Z., Li, W., Zhang, Q., Zhang, C., Yang, W., Liu, Q., Su, N., Lu, Y., Yin, X., Wang, F., Gu, C., Yang, A., Luo, B., Zhou, M., Shen, L., Pan, C., Wang, Z., Wu, Q., Yin, J., Hou, Y., Shi, Y., 2024. Development of fully automated models for staging liver fibrosis using non-contrast mri and artificial intelligence: a retrospective multicenter study. *eClinicalMedicine* 77.
- Li, K., Wang, Y., Zhang, J., Gao, P., Song, G., Liu, Y., Li, H., Qiao, Y., 2023. Uniformer: Unifying convolution and self-attention for visual recognition. *IEEE Transactions on Pattern Analysis and Machine Intelligence (TPAMI)* 45, 12581–12600.
- Li, W., Zhu, Y., de Zhao, G., Chen, X., Zhao, X., Xu, H., Che, Y., Chen, Y., Ye, Y., Dou, X., Wang, H., Cheng, J., Xie, Q., Chen, K., 2025. Deep learning-based automated assessment of hepatic fibrosis via magnetic resonance images and nonimage data. *Quantitative Imaging in Medicine and Surgery* 15, 8250 – 8264.
- Liu, Y., Gao, Z., Shi, N., Wu, F., Shi, Y., Chen, Q., Zhuang, X., 2025a. Merit: Multi-view evidential learning for reliable and interpretable liver fibrosis staging. *Medical Image Analysis* 102, 103507.
- Liu, Y., Zhen, R., Gao, S., Luo, X., Gao, X., Chen, Q., Zhuang, X., 2025b. Bayesmm: Robust deep combined computing tackling heavy-tailed distribution in medical images, in: *Proceedings of the International Conference on Medical Image Computing and Computer Assisted Intervention (MICCAI)*, pp. 45–54.
- Liu, Z., Ning, J., Cao, Y., Wei, Y., Zhang, Z., Lin, S., Hu, H., 2022. Video swin transformer, in: *Proceedings of the IEEE/CVF Conference on Computer Vision and Pattern Recognition (CVPR)*, pp. 3202–3211.
- Lohrke, J., Frenzel, T., Endrikat, J., Alves, F.C., Grist, T.M., Law, M., Lee, J.M., Leiner, T., Li, K.C., Nikolaou, K., et al., 2016. 25 years of contrast-enhanced mri: developments, current challenges and future perspectives. *Advances in therapy* 33, 1–28.
- Macdonald, J.A., Zhu, Z., Konkel, B., Mazurowski, M.A., Wiggins, W.F., Bashir, M.R., 2023. Duke liver dataset: A publicly available liver mri dataset with liver segmentation masks and series labels. *Radiology: Artificial Intelligence* 5, e220275.
- Nowak, S., Mesropyan, N., Faron, A., Block, W., Reuter, M., Attenberger, U.I., Luetkens, J.A., Sprinkart, A.M., 2021. Detection of liver cirrhosis in standard t2-weighted mri using deep transfer learning. *European radiology* 31, 8807–8815.
- Rockey, D.C., Caldwell, S.H., Goodman, Z.D., Nelson, R.C., Smith, A.D., 2009. Liver biopsy. *Hepatology* 49, 1017–1044.
- Roehlen, N., Crouchet, E., Baumert, T.F., 2020. Liver fibrosis: mechanistic concepts and therapeutic perspectives. *Cells* 9, 875.
- Scheuer, P.J., 1991. Classification of chronic viral hepatitis: a need for reassessment. *Journal of hepatology* 13, 372–374.
- Venkatesh, S.K., Yin, M., Takahashi, N., Glockner, J.F., Talwalkar, J.A., Ehman, R.L., 2015. Non-invasive detection of liver fibrosis: Mr imaging features vs. mr elastography. *Abdominal imaging* 40, 766–775.
- Wojciechowska, M., Malacrino, S., Garcia Martin, N., Fehri, H., Rittscher, J., 2021. Early detection of liver fibrosis using graph convolutional networks, in: *Proceedings of the International Conference on Medical Image Computing and Computer Assisted Intervention (MICCAI)*, Springer. pp. 217–226.
- Xue, L.Y., Jiang, Z.Y., Fu, T.T., Wang, Q.M., Zhu, Y.L., Dai, M., Wang, W.P., Yu, J.H., Ding, H., 2020. Transfer learning radiomics based on multimodal ultrasound imaging for staging liver fibrosis. *European radiology* 30, 2973–2983.
- Yasaka, K., Akai, H., Kunimatsu, A., Abe, O., Kiryu, S., 2017. Liver fibrosis: Deep convolutional neural network for staging by using gadoxetic acid-enhanced hepatobiliary phase mr images. *Radiology* 287 1, 146–155.
- Yasaka, K., Akai, H., Kunimatsu, A., Abe, O., Kiryu, S., 2018. Deep learning for staging liver fibrosis on ct: a pilot study. *European Radiology* 28, 4578–4585.
- Yin, C., Liu, S., Lyu, F., Lu, J., Darkner, S., Wong, V.W.S., Yuen, P.C., 2024. Xfibrosis: Explicit vessel-fiber modeling for fibrosis staging from liver pathology images, in: *Proceedings of the IEEE/CVF Conference on Computer Vision and Pattern Recognition (CVPR)*, pp. 11282–11291.
- Zhang, Y., He, N., Yang, J., Li, Y., Wei, D., Huang, Y., Zhang, Y., He, Z., Zheng, Y., 2022. mmformer: Multimodal medical transformer for incomplete multimodal learning of brain tumor segmentation, in: *Proceedings of the International Conference on Medical Image Computing and Computer Assisted Intervention (MICCAI)*, pp. 107–117.
- Zhao, H., Zhang, X., Gao, Y., Wang, L., Xiao, L., Liu, S., Huang, B., Li, Z., 2024. Diagnostic performance of efficientnetv2-s method for staging liver fibrosis based on multiparametric mri. *Heliyon* 10.
- Zheng, T., Zhu, Y., Chen, Y., Mai, S., Xu, L., Jiang, H., Duan, T., Wu, Y., Qu, Y., Chen, Y., et al., 2024. Fully automated mri-based convolutional neural network for noninvasive diagnosis of cirrhosis. *Insights into Imaging* 15, 298.
- Zhuang, X., Ding, W., Liu, Y., Ma, Y., Zhao, J., Wang, B. (Eds.), 2025. *Comprehensive Analysis and Computing of Real-World Medical Images*. Springer.